International Journal of Pharmaceutics 670 (2025) 125160

Contents lists available at ScienceDirect

International Journal of Pharmaceutics

journal homepage: www.elsevier.com/locate/ijpharm

Combination of Apigenin and Melatonin with nanostructured lipid carriers as anti-inflammatory ocular treatment

Lorena Bonilla-Vidal [a,b], Marta Espina [a,b], María Luisa García [a,b], Laura Baldomà [c,d], Josefa Badia [c,d], Anna Gliszczyńska [e], Eliana B. Souto [f], Elena Sánchez-López [a,b,*]

[a] Department of Pharmacy, Pharmaceutical Technology and Physical Chemistry, Faculty of Pharmacy and Food Sciences, University of Barcelona, 08028, Barcelona, Spain
[b] Institute of Nanoscience and Nanotechnology (IN^{2}UB), University of Barcelona, 08028 Barcelona, Spain
[c] Department of Biochemistry and Physiology, Faculty of Pharmacy and Food Sciences, University of Barcelona, 08028, Barcelona, Spain
[d] Institute of Biomedicine of the University of Barcelona (IBUB), Institute of Research of Sant Joan de Déu (IRSJD), 08950 Barcelona, Spain
[e] Department of Food Chemistry and Biocatalysis, Wrocław University of Environmental and Life Sciences, Norwida 25, 50-375 Wrocław, Poland
[f] UCD School of Chemical and Bioprocess Engineering, University College Dublin, Belfield D04 V1W8, Ireland

ARTICLE INFO

Keywords:
Lipid nanoparticles
Apigenin
Melatonin
Dual delivery system
Ocular inflammation
Nanostructured lipid carriers

ABSTRACT

Ocular inflammation is a complex pathology with limited treatment options. While traditional therapies have side effects, novel approaches, such as natural compounds like Apigenin (APG) and Melatonin (MEL) offer promising solutions. APG and MEL, in combination with nanostructured lipid carriers (NLC), may provide a synergistic effect in treating ocular inflammation, potentially improving patient outcomes and reducing adverse effects. NLC could provide chemical protection of these compounds, while offering a sustained release into the ocular surface. Optimized NLC exhibited suitable physicochemical parameters, physical stability, sustained release of APG and MEL, and were biocompatible *in vitro* with a corneal cell line, and *in ovo* by using hen's egg chorioallantoic membrane test. *In vitro* and *in vivo* studies confirmed the NLC' ability to attenuate inflammation by reducing interleukin-6 (IL-6), IL-8 and monocyte chemoattractant protein 1 (MCP-1) cytokine levels and by decreasing inflammation in a rabbit model. These findings suggest that the co-encapsulation of APG and MEL into NLC could represent a promising strategy for managing ocular inflammatory conditions.

1. Introduction

Ocular inflammation constitutes a significant and multifaceted challenge in ophthalmology. Encompassing a spectrum of disorders affecting several ocular structures, from the orbit to the optic nerve, ocular inflammation treatment requires a comprehensive approach involving multiple medical disciplines (Xu and Rao, 2022). The etiology of ocular inflammation is diverse, ranging from infectious and autoimmune processes to vascular and degenerative conditions (Egwuagu et al., 2015). While often considered a secondary manifestation of systemic diseases, such as rheumatoid arthritis or lupus, ocular inflammation can also be a primary disorder with potentially severe consequences, including vision loss (Musa et al., 2024; Artifoni et al., 2013).

The management of ocular inflammation involves substantial therapeutic challenges. Traditionally, corticosteroids and nonsteroidal anti-inflammatory drugs (NSAIDs) have been the first-line treatment (Colin, 2007; Schalnus, 2003), but these agents are associated with significant adverse effects, both locally and systemically (Rigas et al., 2020). The emergence of novel therapeutic strategies, including immunomodulatory and biologic agents, offers promising avenues for improved patient outcomes (Mazet et al., 2020). In order to develop targeted and more effective therapies with these agents, a better understanding of the underlying pathophysiology of ocular inflammatory diseases is instrumental (Lee and Dick, 2011). Recent research has highlighted the role of inflammatory mediators in conditions previously considered non-inflammatory, such as age-related macular degeneration (AMD) and diabetic retinopathy, emphasizing the need for a re-evaluation of treatment paradigms (Starace et al., 2021; Yue et al., 2022).

Among anti-inflammatory molecules, natural compounds constitute an emerging novel therapeutic field. Among them, two compounds stand out: Apigenin (APG), the main flavone of chamomile, and

* Corresponding author.
E-mail address: esanchezlopez@ub.edu (E. Sánchez-López).

https://doi.org/10.1016/j.ijpharm.2024.125160
Received 21 November 2024; Received in revised form 28 December 2024; Accepted 30 December 2024
Available online 31 December 2024

Melatonin (MEL), a neurohormone. APG exhibits potent anti-inflammatory properties primarily by inhibiting the expression of inducible nitric oxide synthase (iNOS) and cyclooxygenase-2 (COX-2), key enzymes in inflammatory pathways (Mushtaq et al., 2023; Yoon et al., 2023). This reduction in pro-inflammatory mediators is attributed to APG ability to suppress the activation of transcription factors, such as nuclear factor κB (NF-κB), responsible for regulating inflammatory gene expression. Additionally, APG antioxidant properties contribute to its anti-inflammatory effects (Ali et al., 2016). MEL, an indoleamine synthesized mainly in the pineal gland, also exhibits potent anti-inflammatory properties. Its antioxidant activity, including direct radical scavenging and induction of antioxidant enzymes, mitigates oxidative stress, a key driver of inflammation (Cho et al., 2021). MEL also modulates inflammatory responses by inhibiting the nuclear translocation of NF-κB, a pivotal transcription factor in the regulation of pro-inflammatory gene expression (Bantounou et al., 2022). Consequently, MEL suppresses the production of cytokines, such as tumor necrosis factor α (TNF-α) and interleukin-6 (IL-6), and adhesion molecules, thereby attenuating inflammatory processes (Zarezadeh et al., 2020). Furthermore, it is well-known that MEL is able to decrease intraocular pressure (IOP), which could counteract the side effects of NSAIDs and corticosteroids (Alkozi et al., 2020). In this way, the combination of APG and MEL to inhibit inflammation via complementary therapeutic pathways, could represent a disruptive therapeutic strategy to treat ocular inflammatory pathologies and also to avoid common adverse effects of conventional treatments. Despite the promising synergistic potential of this combination, the primary limitation is the low bioavailability of both drugs. MEL exhibits poor aqueous solubility, rapid clearance, and susceptibility to photodegradation, while APG suffers from extensive metabolism and low aqueous solubility (Zhang et al., 2012; Lopes et al., 2020).

The ocular surface presents a barrier to drug delivery, characterized by rapid tear turnover, anatomical corneal barrier, enzymatic degradation, and efficient drug efflux. These physiological challenges, coupled with the delicate nature of ocular tissues, significantly hinder the development of effective ophthalmic formulations (Bonilla et al., 2022). Conventional dosage forms, such as solutions and suspensions, often exhibit poor bioavailability due to rapid drainage and precorneal loss. Consequently, frequent administration is required, increasing patient burden and potentially inducing ocular irritation. To address these limitations, nanotechnology-based drug delivery systems have emerged as promising alternatives (Souto et al., 2010; Wong and Wong, 2019). Lipid nanoparticles offer several advantages including enhanced drug solubility, prolonged ocular residence time, and protection from enzymatic degradation. This approach holds the potential to improve therapeutic efficacy, reduce dosing frequency, and minimize adverse effects, ultimately enhancing patient compliance and treatment outcomes (Souto et al., 2010). Furthermore, last generation of lipid nanoparticles, the nanostructured lipid carriers (NLC), also incorporate a liquid lipid, in this case rosehip oil (RHO), which may also reinforce the intrinsic anti-inflammatory and anti-oxidant properties of APG and MEL (Mármol et al., 2017; Belkhelladi and Bougrine, 2024).

Preliminary work documented the potential of NLC to encapsulate APG for dry eye disease (Bonilla-Vidal et al., 2024), and MEL for the treatment of uveal melanoma (Bonilla-Vidal et al., 2024). To combine the potential of both compounds, a novel cationic NLC formulation co-encapsulating APG and MEL was developed. The incorporation of dimethyl dioctadecyl ammonium bromide (DDAB), as a cationic surfactant, aimed at improving the ocular bioavailability of the NLC by promoting electrostatic interactions with the ocular surface characterized by a negatively charged mucosa (Fangueiro et al., 2016). This approach was supported by previous studies demonstrating DDAB safety and efficacy for ocular drug delivery (Silva et al., 2019). The present investigation sought to optimize this cationic NLC formulation for the treatment of ocular inflammation through comprehensive *in vitro* and *in vivo* evaluation of biocompatibility, cytotoxicity, and anti-inflammatory properties *in vitro* and *in vivo*.

2. Materials and methods

2.1. Materials

APG was obtained from Apollo Scientific (Cheshire, UK) and MEL from Thermo Fisher Scientific (Massachusetts, USA). Glyceryl distearate (Compritol® 888 ATO) was supplied by Gattefossé (Madrid, Spain). Nile red (NR) and polysorbate 80 (Tween® 80) were purchased from Sigma-Aldrich (Madrid, Spain). RHO was acquired from Acofarma Fórmulas Magistrales (Barcelona, Spain), and DDAB (dimethyl dioctadecyl ammonium bromide) was obtained from TCI Europe (Zwijndrecht, Belgium). All additional reagents employed were of analytical grade purity. Ultrapure water was generated using a Millipore Milli-Q Plus system.

2.2. Production of APG-MEL-NLC

APG-MEL-NLC were fabricated by the hot high-pressure homogenization using a Homogenizer FPG 12800 (Stansted, UK) previously optimized (Bonilla-Vidal et al., 2023). Briefly, a pre-emulsion was initially formed by subjecting the components to 8000 rpm agitation for 30 s using an Ultraturrax® T25 (IKA, Germany). Subsequent homogenization was conducted under controlled conditions of 85 °C, with three cycles at a pressure of 900 bar. To produce positive surface charged NLC, incremental amounts of the cationic lipid DDAB were integrated into APG-MEL-NLC, as previously described (Bonilla-Vidal et al., 2023).

2.3. Physicochemical characterization

The physical properties – average size (Z_{av}) and polydispersity index (PI) – were characterized by dynamic light scattering (DLS), using a Zetasizer NanoZS (Malvern Instruments, UK) at 25 °C. Samples were diluted 1:10 in Milli-Q water. Zeta potential (ZP) was assessed using the same instrument, by laser-Doppler electrophoresis, with samples diluted 1:20 in Milli-Q water. All measurements were conducted in triplicate (Esteruelas et al., 2021).

Encapsulation efficiency (EE) was calculated indirectly by determining the amount of free APG and MEL in the supernatant after centrifugation of the APG-MEL-NLC dispersion through an Amicon® Ultra 0.5 centrifugal filter device. The free drug concentrations were determined by reverse-phase high performance liquid chromatography (HPLC), and EE calculated based on the difference between the initial drug amount and the free drug content using Eq. (1) (Llorente et al., 2023).

$$EE = \frac{Total\ amount\ of\ APG + MEL - Free\ amount\ of\ APG + MEL}{Total\ amount\ of\ APG + MEL} x100 \quad (1)$$

APG and MEL concentrations were quantified via reverse-phase HPLC. An HPLC Waters 2695 separation module (Waters, Massachusetts, USA) equipped with a Kromasil® C18 column (5 µm, 150 × 4.6 mm) was used for analysis. The mobile phase comprised a water phase containing 2 % acetic acid and an organic phase composed of methanol. A gradient elution was implemented, initiating with 40 % water phase, progressing to 60 % water phase over 5 min, followed by a reverse gradient returning to 40 % water phase in the subsequent 5 min. The flow rate was maintained at 0.9 mL/min. Drug quantifications were performed using a Waters® 2996 diode array detector at 300 nm, with data processed using Empower® 3 Software (Bonilla-Vidal et al., 2023).

2.4. Characterization of the optimized APG-MEL-NLC

2.4.1. Transmission electron microscopy

The morphological properties of the NLC were examined using transmission electron microscopy (TEM) on a JEOL 1010 microscope (Akishima, Japan). Negative staining with 2 % uranyl acetate was performed on UV-activated copper grids to visualize the morphology of APG-MEL-NLC (Galindo et al., 2022).

2.4.2. Interaction studies

Thermal properties of APG-MEL-NLC were characterized using differential scanning calorimetry (DSC) on a Mettler-Toledo DSC 823e System (Barcelona, Spain). The system was calibrated with an indium pan and an empty aluminum pan as reference. Samples were heated from 25 to 105 °C at 10 °C/min under nitrogen atmosphere. Data were analyzed using Mettler STARe V 9.01 dB software. The crystallinity of the samples was evaluated using X-ray diffraction (XRD) with CuKα radiation in the 2θ range of 2° to 60°. Fourier transformed-infrared (FTIR) analysis of APG-MEL-NLC was conducted using a Thermo Scientific Nicolet iZ10 spectrometer equipped with an ATR diamond and a deuterated triglycine sulfate (DTGS) detector (Thiruchenthooran et al., 2022).

2.5. Stability studies

APG-MEL-NLC were subjected to storage at 4, 25, and 37 °C. Stability was assessed by monitoring light backscattering (BS) profiles using a Turbiscan® Lab instrument each month. The experiment endpoint was considered to be the one that showed sample destabilization, confirmed by BS variations higher than 10 %. A glass cell containing 10 mL of sample was utilized, with measurements conducted using a pulsed near-infrared light-emitting diode (λ = 880 nm) and a detector positioned at a 45° angle. The Z_{av}, PI, ZP, and EE were determined simultaneously (Thiruchenthooran et al., 2024).

2.6. In vitro release profile

In vitro release of APG and MEL from NLC formulations was evaluated using Franz-type diffusion cells, with a diffusion area of 0.20 cm^2 and cellulose dialysis membranes (MWCO 12 kDa). Experiments were conducted under previously described conditions (Bonilla-Vidal et al., 2023), using a PBS solution containing 20 % ethanol and 5 % Tween® 80 (pH 7.4) as the receptor medium. NLC formulations were compared to APG and MEL solutions used as controls. Release studies were performed at 37.0 ± 0.5 °C for 48 h. Formulations (300 µL) were applied to the donor compartment, and samples (150 µL) were collected at specific time intervals, and replaced with fresh receptor solution. APG and MEL concentrations in the receptor medium were determined by HPLC, and the cumulative release amounts were computed. Each sample was analyzed in triplicate.

2.7. Ocular tolerance

2.7.1. In vitro study: HET-CAM test and HET-CAM TBS

The hen's egg choriolantoic membrane (HET-CAM) assay was employed to assess the *in vitro* ocular tolerance of APG-MEL-NLC for ophthalmic suitability. Adhering to ICCVAM guidelines, 300 µL of each formulation (free APG/MEL, APG-MEL-NLC, NaOH 0.1 M, and NaCl 0.9 %) were applied to the choriolantoic membrane (CAM) of fertilized chicken eggs (n = 3/group) for 5 min. Signs of irritation, coagulation and hemorrhage were monitored, and the ocular irritation index (OII) was determined using Eq. (2), where H, V and C stand for the time (seconds) to induce hemorrhage (H), vasoconstriction (V), and coagulation (C). Formulations were categorized as non-irritating (OII ≤ 0.9), weakly irritating (0.9 < OII ≤ 4.9), moderately irritating (4.9 < OII ≤ 8.9), or irritating (8.9 < OII ≤ 21) (Sánchez-López et al., 2020).

$$OII = \frac{(301 - H)\cdot 5}{300} + \frac{(301 - V)\cdot 7}{300} + \frac{(301 - C)\cdot 9}{300} \quad (2)$$

To quantify membrane damage, trypan blue staining (TBS) test was applied to the CAM following the HET-CAM assay. The CAM was incubated with 1 mL of 0.1 % TBS for 1 min, then rinsed with distilled water to remove excess dye. Subsequently, the stained CAM was excised, extracted in 5 mL formamide, and the absorbance of the extract measured by spectrophotometric analysis at 595 nm to determine trypan blue incorporation. A calibration curve of TBS in formamide was built to quantify the absorbed dye (Bonilla-Vidal et al., 2024).

2.7.2. In vivo study: Draize test

The implemented experimental *in vivo* methods were performed in compliance with the UB Ethical Committee for Animal Experimentation standards and applicable regulations (Decree 214/97, Gencat). To corroborate HET-CAM results, the Draize primary eye irritation test was performed on male New Zealand albino rabbits (2.0–2.5 kg, San Bernardo farm, Spain). Fifty microliters of each formulation were administered into the conjunctival sac of each animal (n = 3 rabbits/group), followed by gentle massage to facilitate corneal absorption. Irritation indicators (corneal opacity, conjunctival hyperaemia, chemosis, ocular discharge, iris abnormalities) were assessed immediately and also after 1 h, 24 h, 48 h, 72 h, 7 days, and 21 days post-instillation. The untreated contralateral eye functioned as a negative control. Draize scores were allocated according to corneal opacity, iris modifications, and conjunctival changes (hyperaemia, chemosis, swelling, discharge) (Fernandes et al., 2022).

2.8. Cellular experiments

2.8.1. Cell culture

Human corneal epithelial (HCE-2) cells were cultured in keratinocyte serum-free growth medium (SFM; Life Technologies, Invitrogen, GIBCO®, Paisley, UK) supplemented with epidermal growth factor (5 ng/mL), bovine pituitary extract (0.05 mg/mL), penicillin (100 U/mL), insulin (0.005 mg/mL) and streptomycin (100 mg/mL). Cells were incubated in flasks at 37 °C with 10 % CO_2 in a humidified atmosphere until achieving 80 % confluence (26).

2.8.2. Cell viability

The cytotoxicity of APG-MEL-NLC was evaluated using the 3-[4,5-dimethylthiazol-2-yl]-2,5 diphenyl tetrazolium bromide (MTT) test, which quantifies the metabolic activity of viable cells via tetrazolium salt reduction by intracellular dehydrogenases. HCE-2 cells (100 µL, 2×10^5 cells/mL) were seeded in a 96-well plate followed by incubation for 48 h at 37 °C. To simulate corneal conditions, cells were exposed to several sample concentrations (6.67×10^{-4}–5.00×10^{-2} mg/mL of drugs combination) for 5, 15, and 30 min. Following incubation, MTT solution (0.25 % in PBS) was added, and after 2 h replaced with dimethyl sulfoxide. Cell viability was assessed by measuring absorbance at 560 nm using a Modulus® Microplate Photometer, expressed as a percentage of untreated control cells (Bonilla-Vidal et al., 2024; López-Machado et al., 2021).

2.8.3. Determination of proinflammatory cytokines

To assess the anti-inflammatory activity APG-MEL-NLC and free drug combinations, HCE-2 cells were seeded at a density of 2×10^5 cells/mL in 12-well plates and cultured until reaching 90 % confluence. Samples were administered for 30 min incubation at a concentration of 0.02 mg drugs combination/mL, and inflammation was induced with lipopolysaccharide (LPS) at 10 µg/mL. LPS-stimulated cells served as the positive control and untreated cells as the negative control. Moreover, cells with APG-MEL-NLC were also assesed without LPS stimuli. For the inflammation prevention, the formulations were incubated for 30 min, washed

with PBS, and incubated with LPS for 24 h. Following 24 h incubation, supernatants were collected, centrifuged at 16,000 g for 10 min at 4 °C, and stored at –80 °C. For the inflammation treatment, LPS was administered for 24 h, and then the treatments were applied for 30 min. Afterwards, supernatants were processed in the same manner (López-Machado et al., 2021).

The levels of pro-inflammatory cytokines IL-6, IL-8 and monocyte chemoattractant protein 1 (MCP-1) were quantified in the supernatants using Custom human ProcartaPlex Multiplex immunoassays (Labclinics, Barcelona, Spain), according to the manufacturer's protocol, with results analyzed by Luminex MAGPIX® expressed as pg/mL.

2.9. In vivo anti-inflammatory efficacy

All experimental procedures were conformed with the guidelines of the UB Ethical Committee for Animal Experimentation, complying with current regulations (Decree 214/97, Gencat), and received approval under protocol code 326/19. To assess the effects of APG-MEL-NLC against ocular inflammation, New Zealand male albino rabbits (n = 3/group) were used. The samples comprised APG-MEL-NLC, free APG and MEL, and a control solution of 0.9 % NaCl. To evaluate the inflammation preventive effects of APG-MEL-NLC, 50 μL of each sample were applied topically in the right eye, followed by 50 μL of 0.5 % sodium arachidonate (SA) in PBS to induce inflammation 30 min after the samples application. The left eye received no sample and was used as the control. To evaluate the anti-inflammatory effects of APG-MEL-NLC, SA was administered 30 min before application of each sample. Ocular assessments were monitored up to 210 min utilizing a modified Draize scoring system (Bonilla-Vidal et al., 2024; López-Machado et al., 2021).

2.10. Statistical analysis

Data analysis was conducted via GraphPad Prism 9. Two-way ANOVA, followed by Tukey's post-hoc test, was utilized for multiple group comparisons, whereas Student's *t*-test was employed for pairwise comparisons. Data are expressed as mean ± standard deviation (SD), with statistical significance established at $p < 0.05$.

3. Results

3.1. Production of cationic APG-MEL-NLC

The present study used a previously optimized formulation (5.0 % of lipid phase containing 3.25 % of solid lipid, 4.0 % of surfactant, 0.067 % of APG and 0.033 % of MEL) as the starting point. To investigate the influence of the cationic surfactant on the physicochemical properties of APG-MEL-NLC, increasing concentrations of DDAB were added to the formulations (Table 1). The selection of the optimal cationic formulation was based on achieving a ZP exceeding + 15 mV and a PI below 0.3. According to these parameters, the formulation containing 0.06 % DDAB was determined to be optimal.

3.2. Characterization of optimized APG-MEL-NLC

TEM analysis revealed that APG-MEL-NLC are predominantly spherical with a mean diameter below 200 nm (Fig. 1A). These results are corroborated by the data recorded by DLS. No evidence of particle aggregation was observed.

FTIR spectroscopy was used to investigate the molecular interactions among the drugs, surfactant, and lipid matrix (Fig. 1B). The FTIR spectrum of APG exhibited characteristic peaks at approximately 3278, 2800, 1650 and 1605 cm^{-1}, attributed to O–H, C–H, and C-O functional groups, respectively. MEL displayed distinct peaks at 3303, 1629, 1555 and 1212 cm^{-1}, corresponding to N–H, C═O, C-O and C-N groups, respectively. FTIR spectra of APG-MEL-NLC exhibited a prominent absorption band centered at 1100 cm^{-1}, indicative of the presence of the surfactant (Fu et al., 2015). Notably, no new intense bands were observed in APG-MEL-NLC, suggesting the absence of significant covalent bond formation. Additionally, the reduced or absent peaks of APG and MEL support the encapsulation of both drugs within the lipid matrix.

DSC analysis was employed to evaluate alterations in the crystallinity and melting behavior of the bulk materials, their mixtures and of APG-MEL-NLC (Fig. 1C). The melting temperature (T_m) of the lipid mixture was similar to the drug-loaded lipid mixture (69.50 °C). T_m of APG-MEL-NLC was lower than that of the physical lipid mixture (67.59 °C), potentially attributed to their reduced particle size and presence of surfactant (Bunjes et al., 1996). Enthalpy values (ΔH) were comparable for the lipid mixture and drug + lipid mixture (74.1 Jg^{-1} vs. 79.2 Jg^{-1}), whereas APG-MEL-NLC exhibited a lower ΔH (55.4 Jg^{-1}). Thermograms of APG and MEL revealed significantly higher T_m and ΔH values (365.50 °C, 198.50 Jg^{-1} and 118.52 °C, 134.70 Jg^{-1}, respectively), suggesting greater crystallinity and melting points compared to the lipid mixtures.

XRD patterns (Fig. 1D) provided insights into the physical state of the drugs within the NLC. APG, MEL, and the lipid mixture exhibited crystalline profiles, as evidenced by the presence of sharp, intense peaks in their respective XRD spectra. A reduction in peak intensity of MEL diffraction angles (16.34, 20.44 and 26.14°) within the APG-MEL-NLC profile, together with small APG peaks (7.02, 11.25 and 15.95°), suggests that both drugs were solubilized within the lipid matrix, consistent with EE data. The crystallinity of other formulation components was also evaluated. The bulk lipid and drug-loaded lipid mixture displayed prominent peaks at 19.36° (2θ) i.e. $d = 0.46$ nm, indicative of the stable β-form of triacylglycerols. Additionally, two distinct peaks at 21.36° (2θ) i.e. $d = 0.42$ nm and 23.59° (2θ) i.e. $d = 0.38$ nm were attributed to the β'-form of triacylglycerols. APG-MEL-NLC also exhibited these characteristic signals, corresponding to the most common polymorphic forms of triacylglycerols (Souto et al., 2006; Freitas and Müller, 1999).

3.3. Stability studies

Stability of APG-MEL-NLC was assessed by monitoring changes in Z_{av}, PI, ZP, and EE over time. Additionally, BS profiles were recorded for samples stored at 4, 25, and 37 °C to detect risk of destabilization processes, such as sedimentation, agglomeration, or aggregation, indicated by BS variations exceeding 10 % (Fig. 2). The experimental endpoint was stabilized as the day in which the formulation showed any sign of instability. APG-MEL-NLC exhibited stability for 3 months at 4 °C, maintaining consistent physicochemical properties. At 25 °C, stability was observed for 1 month, whereas at 37 °C, the formulation showed stability for only 15 days.

Higher temperatures were associated with accelerated particle destabilization, characterized by neutralization of ZP, because the kinetic energy of the particles increases with temperature, triggering collisions leading to formation of agglomerates (Freitas and Müller,

Table 1
Effect of cationic lipid on the physicochemical parameters.

DDAB (%)	Z_{av} ± SD (nm)	PI ± SD	ZP ± SD (mV)	EE APG ± SD (%)	EE MEL ± SD (%)
0.05	187.5 ± 0.5	0.211 ± 0.008	11.4 ± 0.2	99.9 ± 0.1	54.9 ± 0.4
0.06	166.2 ± 2.4	0.265 ± 0.007	16.8 ± 0.7	99.9 ± 0.1	54.5 ± 0.2
0.07	148.3 ± 1.3	0.299 ± 0.016	15.3 ± 0.5	99.8 ± 0.1	55.1 ± 1.0

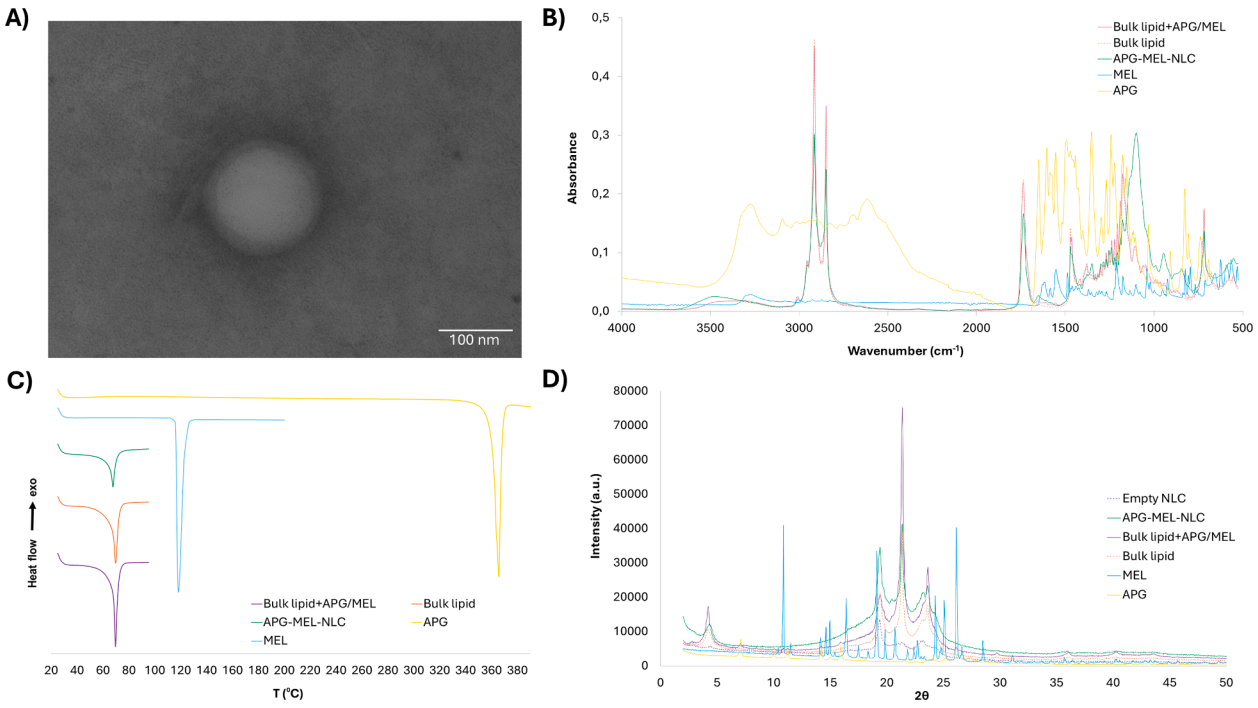

Fig. 1. Characterization of APG-MEL-NLC and their components. (A) TEM image (scale bar 100 nm), (B) FTIR analysis, (C) DSC curves, (D) XRD patterns.

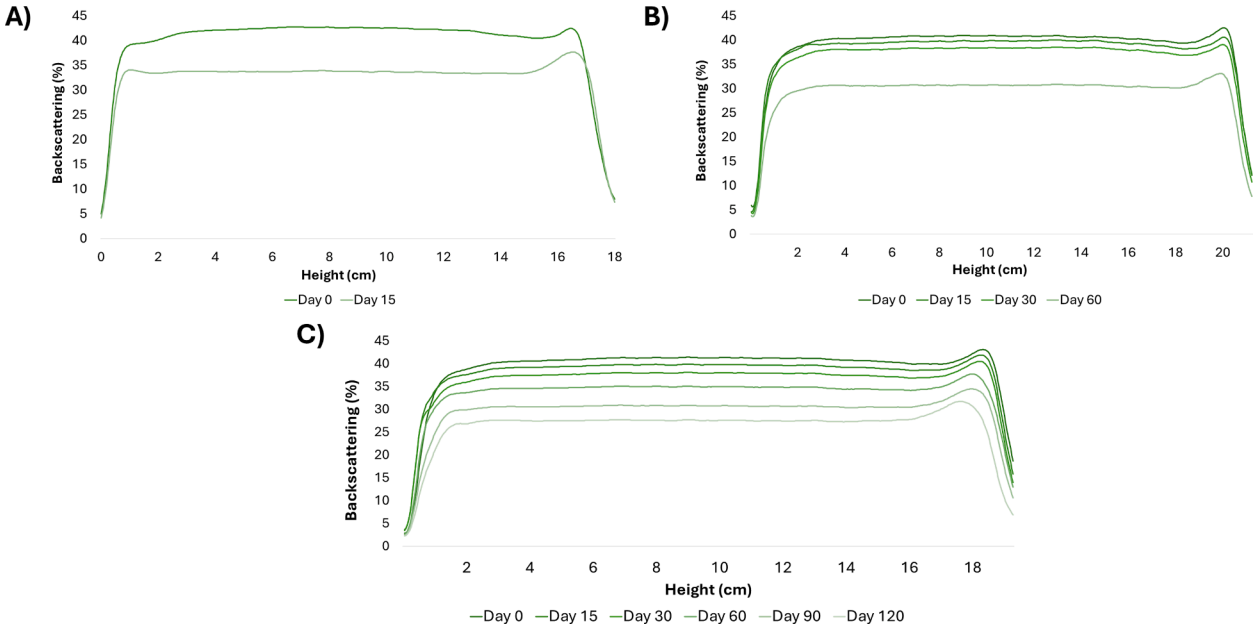

Fig. 2. Backscattering profiles of APG-MEL-NLC stored at (A) 37 °C; (B) 25 °C; and (C) 4 °C.

1998). As indicated in Table 2, the nanoparticles maintained their physicochemical properties until a decrease in ZP was observed at 25 and 37 °C, or a decrease in Z_{av} at 4 °C. These alterations were also in correlation with the BS profiles. In all the cases, destabilization was observed, as highlighted by the 10 % BS difference in the profiles; the data collectively suggest that APG-MEL-NLC stored at 4 °C exhibited higher stability for up to 3 months.

3.4. *In vitro release profile*

In vitro release profiles of APG and MEL from APG-MEL-NLC were compared to their respective free drug counterparts to characterize the drug release kinetics from the particles.

As depicted in Fig. 3, APG release from APG-MEL-NLC exhibited a biphasic pattern adjusted to a two-phase kinetic model. An initial rapid release, likely attributed to APG diffusion from the NLC outer lipid layer, was followed by a sustained release associated with APG release from the inner lipid core. In contrast, free APG showed a complete release within 24 h, adjusted to an exponential plateau model. APG-MEL-NLC released approximately 30 % of their APG content over the same period. Kinetic analysis revealed a lower dissociation constant (K_d) and a longer half-life ($t_{1/2}$) for the sustained release of APG from NLC compared to free APG.

MEL release from APG-MEL-NLC followed a biphasic pattern with an

Table 2
Physicochemical parameters of APG-MEL-NLC stored at different temperatures.

Temperature (°C)	Day	Z_{av} ± SD (nm)	PI ± SD	ZP ± SD (mV)	EE APG ± SD (%)	EE MEL ± SD (%)
	0	160.4 ± 1.6	0.217 ± 0.018	16.1 ± 0.5	99.9 ± 0.1	55.9 ± 0.5
37	15	135.1 ± 1.9	0.201 ± 0.002	11.4 ± 0.4	99.7 ± 0.3	54.2 ± 0.8
25	15	156.0 ± 1.2	0.175 ± 0.014	15.7 ± 0.3	99.9 ± 0.1	53.8 ± 0.4
	30	157.8 ± 2.3	0.189 ± 0.006	13.7 ± 0.3	99.3 ± 0.3	54.1 ± 0.2
	60	147.9 ± 1.0	0.189 ± 0.011	13.1 ± 1.1	99.9 ± 0.1	55.1 ± 0.2
4	15	159.6 ± 1.1	0.199 ± 0.007	15.8 ± 0.8	99.9 ± 0.1	55.7 ± 0.4
	30	160.2 ± 5.0	0.173 ± 0.003	15.0 ± 1.3	99.9 ± 0.1	54.9 ± 0.7
	60	157.8 ± 2.1	0.185 ± 0.019	15.9 ± 0.6	99.8 ± 0.2	55.0 ± 0.3
	120	139.1 ± 0.6	0.200 ± 0.010	15.0 ± 0.8	99.9 ± 0.1	54.1 ± 0.9

initial faster release compared to free MEL. Free MEL was completely released within 24 h, approximately 75 % of encapsulated MEL within the same timeframe was released. Determined parameters demonstrated a lower K_d and a higher $t_{1/2}$ for MEL from NLC than free MEL, indicating a sustained release profile.

3.5. Ocular tolerance

Ocular tolerance was assessed *in vitro* via the HET-CAM assay (Fig. 4) and *in vivo* through the Draize test . The HET-CAM test revealed that 1 M NaOH, serving as a positive control, caused significant haemorrhage that intensified over a 5-minute observation period, indicating a potent irritant. The negative control (0.9 % NaCl), along with both loaded and empty NLC, as well as the free medicines, did not induce any irritating responses on the CAM, categorizing them as non-irritant (OII 0.07 ± 0.01). These findings were corroborated by quantitative TBS analysis, which confirmed the non-irritant nature of APG-MEL-NLC. Because of the limitations of *in vitro* models in predicting *in vivo* ocular tolerance, Draize tests were conducted with free APG and MEL, and APG-MEL-NLC. Results indicated that none of the tested formulation induced ocular irritation *in vivo*. Collectively, these data support the conclusion that APG-MEL-NLC show ocular tolerance, being therefore suitable for further anti-inflammatory studies.

3.6. Cellular experiments

3.6.1. Cell viability

The cytotoxicity of various concentrations of free APG and MEL, APG-MEL-NLC, and empty NLC was assessed on HCE-2 corneal epithelial cells. This cell line was selected to simulate the *in vivo* contact between the formulations and the cornea following topical administration (Mofidfar et al., 2021). Cell viability was evaluated 5, 15, and 30 min after incubation to mimic real exposure conditions. According to ISO 10993–5, cell viability exceeding 80 % indicates no cytotoxicity, while values between 60 % and 80 %, 40 % and 60 %, and below 40 % correspond to weak, moderate, and strong cytotoxicity, respectively (López-García et al., 2014). Results demonstrated that free drug solution (MEL + APG) did not induce significant cytotoxic effects (≥80 %

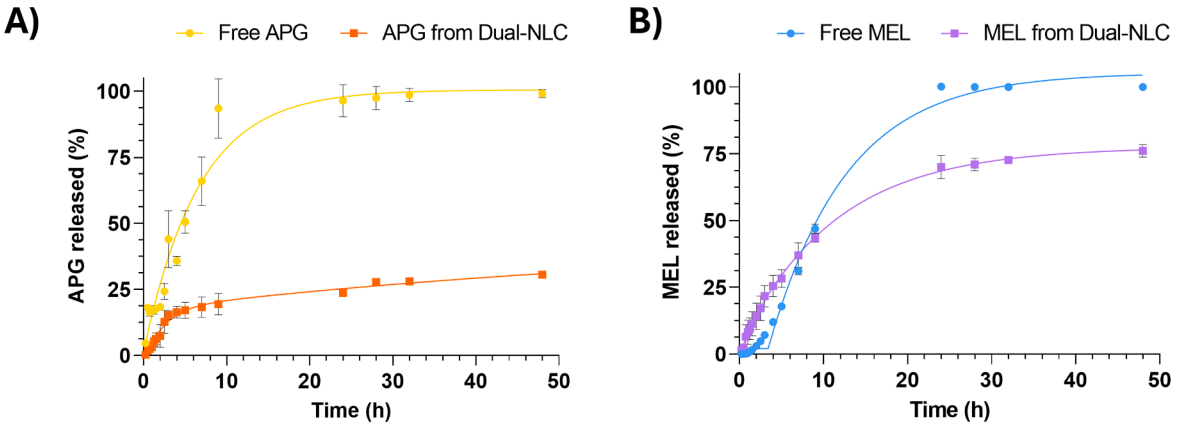

C)

	K_d (h^{-1})	$t_{1/2}$ (h)	*Plateau* (%)	r^2
Free APG	0.1507	4.965	100.5	0.9486
APG from APG-MEL-NLC	$K_{d\ fast}$=0.4340 $K_{d\ slow}$=0.0134	$t_{1/2\ fast}$=1.597 $t_{1/2\ slow}$=51.740	45.9	0.9450
Free MEL	0.1080	6.418	105.4	0.9945
MEL from APG-MEL-NLC	$K_{d\ fast}$=1.2920 $K_{d\ slow}$=0.0885	$t_{1/2\ fast}$=0.537 $t_{1/2\ slow}$=7.836	77.5	0.9863

Fig. 3. *In vitro* release profile of APG and MEL from APG-MEL-NLC vs free APG and MEL carried out for 48 h and adjustment to a two-phase association, two-phase association, exponential Plateau, and Plateau followed by one phase decay model respectively. (A) APG release profile from APG-MEL-NLC. (B) MEL release profile from APG-MEL-NLC. (C) Release calculated parameters: dissociation constant (K_d), half-life ($t_{1/2}$), plateau and correlation coefficient (r^2).

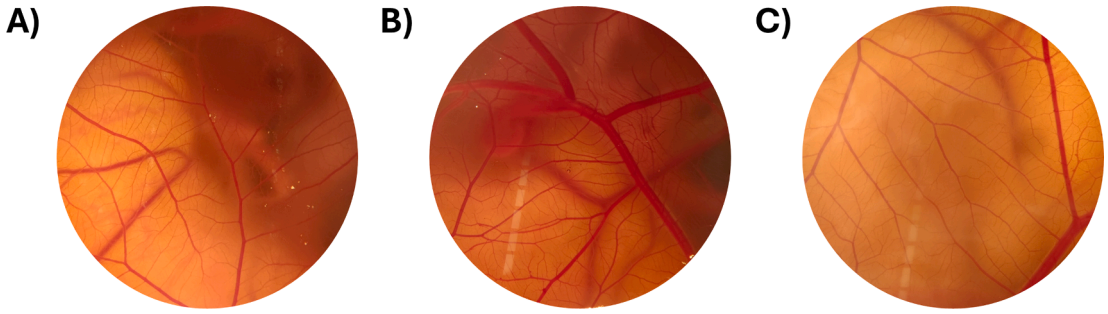

Fig. 4. *In vitro* irritation assay. (A) Negative control, NaCl 0.9 %, (B) Free APG + MEL and (C) APG-MEL-NLC at optimized concentration of 0.67 % APG and 0.33 % MEL.

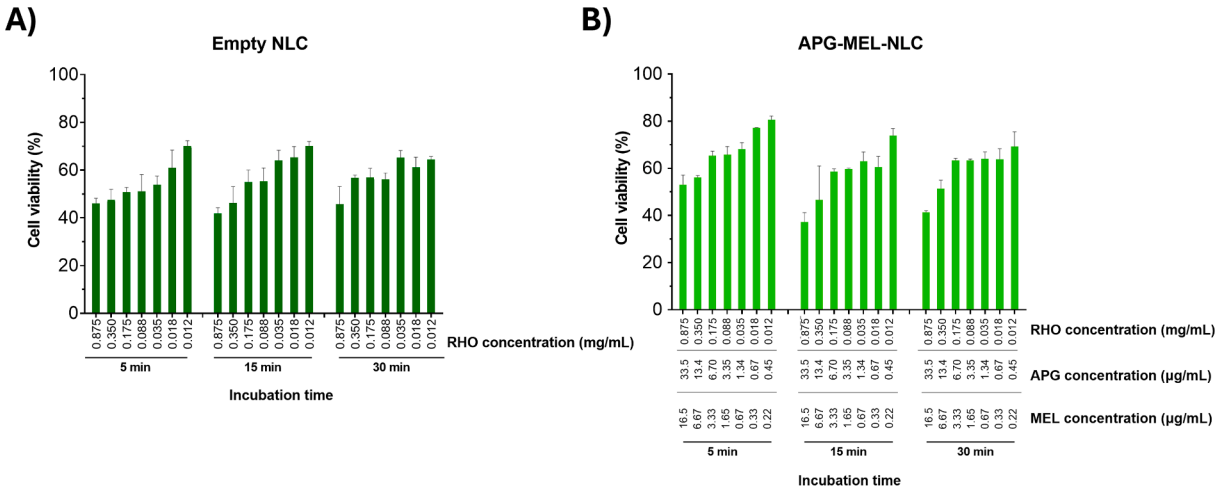

Fig. 5. Cell viability assays. Effect APG-MEL-NLC and empty NLC on the viability of HCE-2 cells at 5, 15 and 30 min. Free drug solution did not induce cytotoxicity at any concentration (≥ 80 % viability).

viability) at any concentration or incubation timepoint. Both formulations showed a moderate toxicity in the highest tested concentration (0.05 mg/mL of total drug concentration). When increasing the dilution, the formulations became less toxic to the cells, but with higher incubation time, the formulations were slightly more toxic (Fig. 5A). However, it can be observed that APG-MEL-NLC were safer (higher cell viability) in all the studied concentrations than empty NLC (Fig. 5B).

3.6.2. *Anti-inflammatory activity of nanoparticles in HCE-2 cells*

The anti-inflammatory potential of the NLC was assessed *in vitro* by evaluating their ability to inhibit LPS-induced cytokine secretion in HCE-2 cells in a prevention and treatment model. The conditions were selected from the results obtained in the cell viability testing, which were the concentration of the free drugs at 6.67 and 3.33 µg/mL of APG and MEL, respectively during 30 min of incubation time.

IL-6, IL-8 and MCP-1 were selected as inflammatory markers. LPS stimulation resulted in significantly elevated levels of cytokines. In the treatment of inflammation, when the tested formulations were applied after LPS stimulus, free drug solution was not able to reduce the inflammatory response, but APG-MEL-NLC were able to significantly inhibit the secretion of the cytokines (Fig. 6A-6C). In the study of the APG-MEL-NLC capacity to prevente inflammation, in which the formulation was applied 30 min incubation before LPS stimulation, the free drugs and APG-MEL-NLC were not able to reduce IL-6 and IL-8 cytokines, but they decreased significatively the MCP-1 levels (****$p < 0.001$) (Fig. 6D-6F).

3.7. *Anti-inflammatory efficacy*

To assess the *in vivo* anti-inflammatory potential of APG-MEL-NLC, their prophylactic and therapeutic efficacy in an ocular inflammation model was evaluated.

The therapeutic efficacy of APG-MEL-NLC was determined by administering treatment 30 min post-inflammatory stimuli. Inflammation severity was monitored over time. Fig. 7A shows a significant reduction in inflammation within 30 min post APG-MEL-NLC administration. Furthermore, the combination of both drugs also induced a significant reduction of inflammation in the first 30 min. In all the monitored times, APG-MEL-NLC showed a significant anti-inflammatory effect.

The preventive capacity of NLC against inflammation was also investigated. APG-MEL-NLC or the free drugs were administered 30 min prior the induction of ocular inflammation. Subsequent inflammation severity was evaluated. Fig. 7B illustrates a significant reduction in inflammation following exposure to the inflammatory stimulus compared to untreated control. In this study, also both treatments showed a significant anti-inflammatory effect, in which APG-MEL-NLC showed a higher activity.

4. Discussion

A cationic NLC containing RHO was formulated to co-encapsulate APG and MEL. The negatively charged corneal mucus layer presents a barrier for drug delivery (Vedadghavami et al., 2020). For this reason, this study aimed to modify a previous formulation by incorporating a cationic surfactant (DDAB) to revert surface charge, potentially

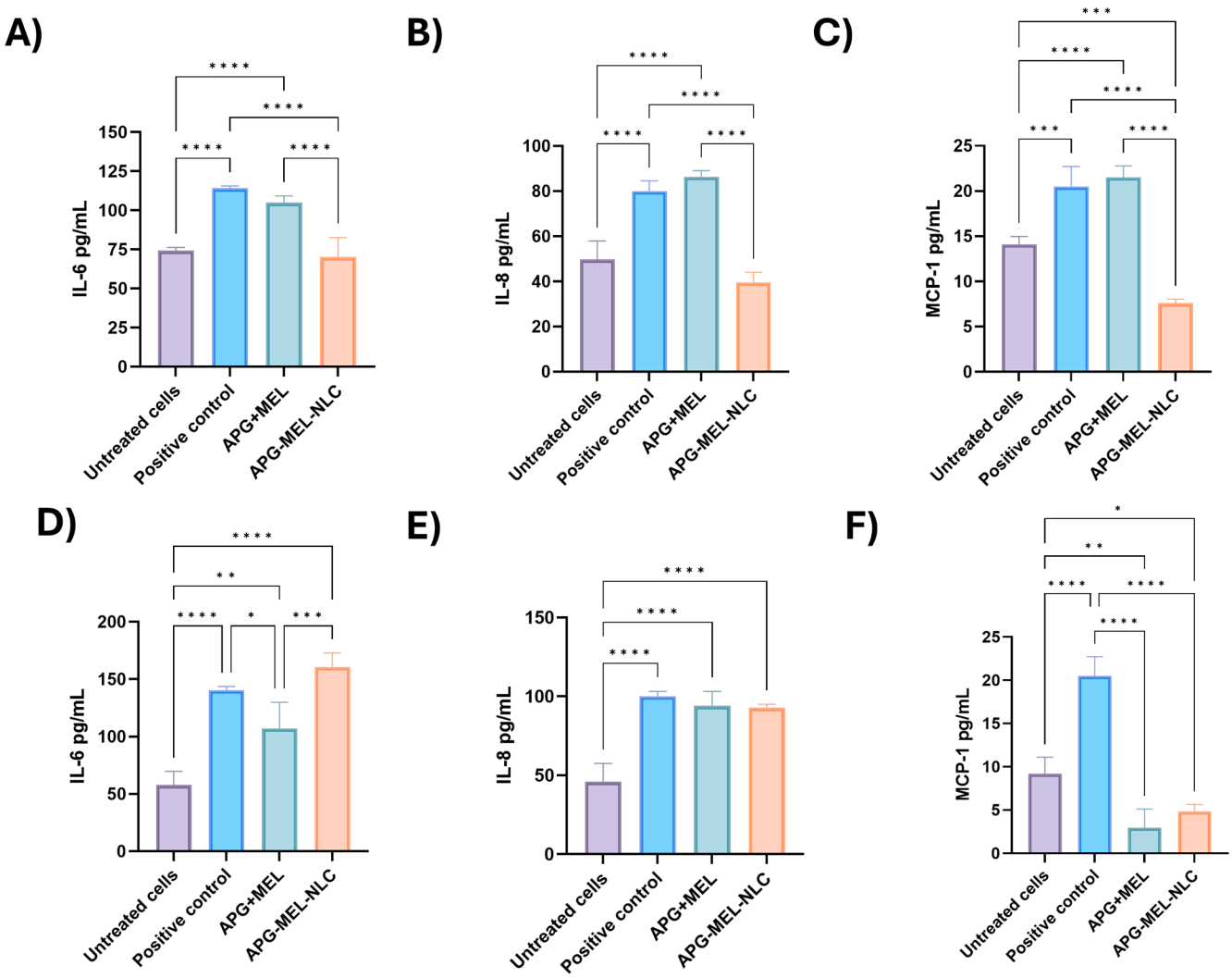

Fig. 6. (A) Quantification of secreted IL-6 proinflammatory cytokine in LPS-stimulated HCE-2 cells in inflammation treatment; (B) Quantification of secreted IL-8 inflammation treatment. (C) Quantification of secreted MCP-1 inflammation treatment; (D) Quantification of secreted IL-6 proinflammatory cytokine in LPS-stimulated HCE-2 cells in inflammation prevention; (E) Quantification of secreted IL-8 inflammation prevention. (F) Quantification of secreted MCP-1 inflammation prevention. Negative control: no treatment; Positive control: LPS. Tested samples were diluted up to 13.4 **μg/mL APG and 6.67 μg/mL MEL**. Results are expressed as the mean ± SD with statistically significant differences (***p < 0.005 and ****p < 0.001).

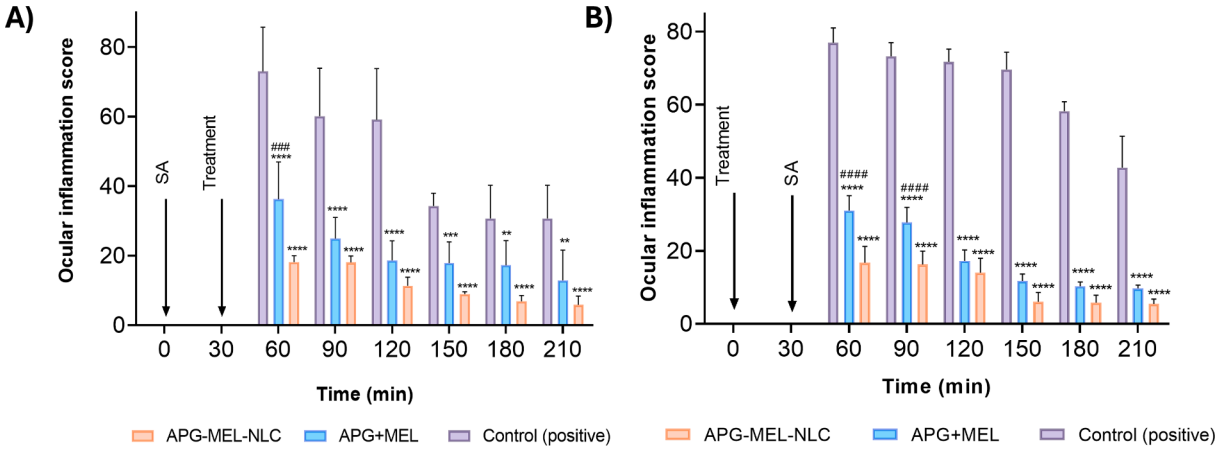

Fig. 7. Comparison of ocular anti-inflammatory efficacy of free APG/MEL and APG-MEL-NLC at the optimized concentration of 0.67 % APG and 0.33 % MEL. (A) Inflammation treatment, (B) inflammation prevention. Values are expressed as mean ± SD; **p < 0.01, ***p < 0.005, and ****p < 0.001 significantly lower effect of the tested formulation than the inflammatory effect induced by SA; ###p < 0.005 and ####p < 0.001 significantly lower effect of APG-MEL-NLC than the free drugs.

enhancing mucoadhesion to the ocular mucosa and subsequently improving bioavailability following topical administration (Abruzzo et al., 2021). Besides the cationic charge of the NLC, it is expected to obtain an enhanced and synergistic effect with the RHO contained in the lipid matrix, which has been described as an anti-inflammatory active (Belkhelladi and Bougrine, 2024; Bonilla-Vidal et al., 2024; Strugała et al., 2016).

To optimize DDAB concentration, the surfactant was incrementally added to a previously optimized formulation (Bonilla-Vidal et al., 2024). Z_{av} remained relatively below 200 nm, whereas the PI increased at higher DDAB concentrations. ZP did not increase with concentrations of DDAB from 0.06 to 0.07 %, remaining at ≈16 mV, and EE was stable in all the tested concentrations. In this way, a DDAB concentration of 0.06 % was selected, yielding a PI below 0.3 and a ZP of approximately 17 mV, achieving suitable physicochemical parameters (Bonilla et al., 2022).

Interaction studies revealed an enhancement of lipid matrix amorphism upon APG and MEL incorporation, suggesting their loading within the lipid matrix of NLC (Ojo et al., 2020). FTIR analysis confirmed the absence of covalent bonds between both drugs and the lipid matrix, indicating that non-covalent interactions, commonly hydrogen bonding and hydrophobic forces, were predominantly responsible for APG and MEL encapsulation within the NLC. This interaction facilitated the sustained release profile of APG and MEL from the particles (Huang et al., 2020). DSC analysis of APG-MEL-NLC revealed a significantly lower melting point compared to the bulk lipid. This suggests a highly amorphous state, possibly attributed to the incorporation of the drugs within the amorphous lipid matrix (Khosa et al., 2018). In comparison to the negatively charged NLC (Bonilla-Vidal et al., 2024), the T_m values were slightly higher with a similar ΔH, which could be attributed to a greater crystallinity of the present formulation. This fact was also observed in previous studies encapsulating MEL, in which the positively charged formulation showed a higher degree of crystallinity, and consequently, a lower stability (Bonilla-Vidal et al., 2024). XRD patterns exhibited characteristic diffraction peaks corresponding to the β and β' polymorphic forms of triacylglycerols (Souto et al., 2006; Zimmermann et al., 2005). In comparison to the previous negatively charged NLC (Bonilla-Vidal et al., 2024), the present formulation showed the two main forms of triacylglycerols, the stable (β) and the metastable (β') ones, which could be related to the slightly lower stability of the particles. Moreover, the formulations encapsulating each compound alone showed higher stability, which could be mainly attributed to the more neutral ZP of the APG-MEL-NLC (+21 mV for APG-NLC and +20 mV for MEL-NLC), but could also be related to the lower concentration of lipid phase in the dual loaded NLC (5 % in APG-MEL-NLC vs 7.5 % in APG-NLC and MEL-NLC). In the case of MEL-NLC (Bonilla-Vidal et al., 2024), it was also observed that the stability of the positively charged formulation presented a reduced stability in comparison to the negatively one, which could be related to the increased crystallinity of the NLC when DDAB was incorporated.

APG-MEL-NLC showed a slow-release profile compared to a rapid diffusion observed for the drugs in solution. The release kinetics of APG-MEL-NLC were best described by a two-phase association model, indicative of a biphasic release pattern. This pattern was characterized by an initial burst release phase followed by a sustained release period, during which approximately 30 and 75 % of the encapsulated APG and MEL respectively were released into the receptor medium. The observed biphasic behavior suggests that the NLC formulation effectively encapsulate APG and MEL, while simultaneously allowing their gradual diffusion through the nanoparticle matrix. In comparison to the release studies performed with MEL negatively charged formulation (Bonilla--Vidal et al., 2024), the positively charged APG-MEL-NLC showed a slower APG release but a faster MEL diffusion, the latter probably due to the modification of the release media. Both actives were able to achieve a higher *plateau* (34.5 % for APG and 76.6 % for MEL in the negatively charged NLC, vs 45.9 % for APG and 77.5 % for MEL in the positively charged NLC). In the case of APG, this slower release from the positively charged NLC has been described by other authors (Wang et al., 2006; Baspinar and Borchert, 2012). Wang et al. (Wang et al., 2006) related this effect to the long carbon chains of the cationic surfactant, which could form an ordered close packing and strengthening the interfacial layer in the particles. In the case of MEL, other authors also found a faster release from a positively charged formulation, in comparison to a negatively and neutrally charged lipid nanoparticle (Landh et al., 2020). In contrast, in comparison to the formulations containing each compound by itself, the co-encapsulation of APG and MEL resulted in a slower release of both compounds. This difference could be related to the lower concentration of each compound in the dual-loaded NLC or to the lowest concentration of lipids (Bonilla-Vidal et al., 2024; Bonilla-Vidal et al., 2024).

To evaluate the ocular safety profile of the formulation, a combination of *in vitro* and *in vivo* assessments was conducted. The *in vitro* HET-CAM assay showed no irritation phenomena following direct application of APG-MEL-NLC. Posterior quantitative analysis of trypan blue uptake corroborated these findings, indicating no toxicity. Subsequently, an *in vivo* ocular irritation study using the Draize test was performed. Results revealed no clinically significant ocular irritation or hyperemia in animals treated with either free APG/MEL or APG-MEL-NLC, suggesting suitable ocular tolerance of the formulation.

The *in vitro* cytotoxicity assays showed that a solution of APG and MEL exhibited no toxic effects on corneal cells across the tested concentration range. Empty NLC showed moderately toxicity the majority of the assessed concentrations. The cationic nature of the particles may contribute to enhanced electrostatic interactions with the negatively charged cell membrane, potentially inducing oxidative stress and subsequent reactive oxygen species (ROS) generation (Yang et al., 2021). Additionally, the lipid composition of the NLC exhibits affinity for cellular membranes, promoting strong interactions (Bonilla et al., 2022; Zhang et al., 2014). Nevertheless, APG-MEL-NLC demonstrated a favorable safety profile across a range of concentrations, except for moderate toxicity observed at the highest tested dose. This protective effect could be related to the properties of the drugs. Jung (Jung, 2014) reported that APG attenuated H_2O_2-induced downregulation of PI3K, AKT2, and ERK2, essential components of cell survival signaling. Concurrently, APG stimulated the expression of antioxidant enzymes SOD1, SOD2, and GPx1. These findings suggested that APG induces their protective effects by counteracting oxidative stress and restoring cellular redox balance. Cavelier et al. (Cavalier et al., 2024) showed that APG can suppress inflammation-related gene and protein expression. It has been widely described that MEL induces their antioxidant effects by stimulating enzymatic defenses within cells, safeguarding mitochondrial membrane phospholipids from oxidative damage, thereby preserving membrane integrity. Additionally, this indolamine influences mitochondrial membrane potential, contributing to its overall protective role in cellular homeostasis, and regulates inflammation processes (Gu et al., 2024; Tarocco et al., 2019; Kopustinskiene and Bernatoniene, 2021). In this way, the initial burst of both drugs could contribute to their fast protective effects in HCE-2 cells.

IL-6, IL-8, and MCP-1 are key inflammatory mediators implicated in ocular diseases. IL-8 primarily recruits neutrophils and eosinophils, while MCP-1 attracts monocytes and lymphocytes (Kany et al., 2019). Both chemokines are upregulated in various ocular inflammatory conditions and contribute to monocyte infiltration (Ghasemi et al., 2011). IL-6, a pleiotropic cytokine involved in inflammation and hematopoiesis, is also upregulated in these settings. These cytokines exhibit synergistic effects, with IL-8 and MCP-1 promoting inflammation and angiogenesis, while IL-6 amplifies inflammatory responses (Da Cunha et al., 2018). Collectively, they play pivotal roles in the pathogenesis of ocular disorders characterized by chronic inflammation and neovascularization. In this way, the *in vitro* anti-inflammatory potential was evaluated by analyzing these three pro-inflammatory cytokines. In the

treatment assay, the results showed that in 30 min exposure to inflamed human corneal cells, APG-MEL-NLC were able to revert LPS-induced inflammation levels in comparison to the free combined drugs. Probably, this strong anti-inflammatory activity of the NLC was related to the interactions of the lipid matrix with the cellular membrane, enhancing the uptake of the formulation in comparison to the free drugs, facilitating their therapeutical action (Mahor et al., 2023). Other authors found that APG was able to reduce IL-6, IL-8 and MCP-1 cytokine levels in different cell lines (Wang et al., 2012; Funakoshi-Tago et al., 2011). In the case of MEL, it has also been described that the neurohormone was able to reduce the levels of the same cytokines (Cho et al., 2021; Deng et al., 2020). However, the prevention results showed that APG-MEL-NLC and the combination of free drugs were not able to decrease IL-6 and IL-8 levels. This fact could be related to the exposure of the treatments to the cells, during which the cells were already inflamed and their membrane could be more permeable, promoting a higher uptake of NLC facilitating their action (Aguilar-Briseño et al., 2020).

Finally, to corroborate *in vitro* experiments, an *in vivo* inflammation assay was performed to evaluate both, inflammation prevention and treatment. The results showed that APG-MEL-NLC possessed a faster and more effective anti-inflammatory properties than the free combination drugs. In the inflammation treatment, during the first 30 min post-instillation, APG-MEL-NLC were able to reduce significantly ocular inflammation, which correlated with the *in vitro* results. Furthermore, in the inflammation prevention, APG-MEL-NLC also showed promising results, decreasing the ocular inflammation score after 30 min. As *in vivo* processes are more complex than *in vitro* ones, both experiments are needed to corroborate the possible therapeutical properties of a formulation. Single loaded nanoparticles (APG-NLC and MEL-NLC) were also tested in previous studies (Bonilla-Vidal et al., 2024; Bonilla-Vidal et al., 2024). Free APG showed a faster and higher anti-inflammatory effect on the inflammation prevention, while free MEL showed the same effect in the inflammation treatment. In the present study, the combination of both drugs acted in a faster way, which could be related to the faster release of MEL in the burst initial phase, and the higher amount of each drug released in each timepoint. It is well-documented that both compounds possess a promising anti-inflammatory activity *in vivo*. Benedeto et al. (Benedeto-Stojanov et al., 2024) described that in an *in vivo* model, MEL prevented an LPS-induced increase in pro-inflammatory cytokines TNF-α and IL-6 and NF-κB levels. Moreover, APG was able to reduce NF-κB and STAT3 activity, inhibiting the inflammation process (Ai et al., 2017).

5. Conclusions

NLC loading APG and MEL showed promising activity as a potential therapeutic tool for ocular inflammation. The formulation exhibited physical stability and sustained release of both encapsulated drugs. *In vitro* and *in vivo* assessments confirmed suitable biocompatibility of the NLC, with no evidence of ocular irritation. Moreover, NLC-mediated delivery of APG and MEL effectively attenuated inflammation *in vitro* by reducing IL-6, IL-8 and MCP-1 cytokine levels and *in vivo* by decreasing the SA inflammation in a rabbit model. These findings collectively suggest that the developed NLC formulation represents a promising strategy for the management and prevention of ocular inflammatory conditions.

CRediT authorship contribution statement

Lorena Bonilla-Vidal: Writing – original draft, Methodology, Investigation, Formal analysis. **Marta Espina:** Writing – review & editing, Supervision, Investigation. **María Luisa García:** Writing – review & editing, Methodology, Investigation, Funding acquisition. **Laura Baldomà:** Writing – review & editing, Methodology, Investigation, Funding acquisition. **Josefa Badia:** Writing – review & editing, Methodology, Investigation, Funding acquisition. **Anna Gliszczyńska:** Writing – review & editing, Methodology, Investigation. **Eliana B. Souto:** Writing – review & editing, Methodology, Investigation, Formal analysis. **Elena Sánchez-López:** Writing – review & editing, Supervision, Methodology, Investigation, Funding acquisition, Formal analysis.

Funding

This research was supported by the Spanish Ministry of Science and Innovation (PID2021-122187NB-C32) and by the Fons d'Impuls per a la Innovació (F2I-PdCl-2024-012).

Declaration of competing interest

The authors declare that they have no known competing financial interests or personal relationships that could have appeared to influence the work reported in this paper.

Acknowledgements

E.S.-L. wants to acknowledge the support of the Grants for the Requalification of the Spanish University System.

Data availability

Data will be made available from corresponding authors upon reasonable request.

References

Abruzzo, A., Giordani, B., Miti, A., Vitali, B., Zuccheri, G., Cerchiara, T., et al., 2021. Mucoadhesive and mucopenetrating chitosan nanoparticles for glycopeptide antibiotic administration. Int. J. Pharm. 606, 120874.
Aguilar-Briseño, J.A., Moser, J., Rodenhuis-Zybert, I.A., 2020. Permeability of endothelium. Curr. Opin. Virol. 43, 41–49.
Ai, X.Y., Qin, Y., Liu, H.J., Cui, Z.H., Li, M., Yang, J.H., et al., 2017. Apigenin inhibits colonic inflammation and tumorigenesis by suppressing STAT3-NF-κB signaling. Oncotarget 8 (59), 100216.
Ali, F., Rahul, N.F., Jyoti, S., Siddique, Y.H., 2016. Health functionality of apigenin: a review. Int. J. Food Prop. 20 (6), 1197–1238.
Alkozi, H.A., Navarro, G., Franco, R., Pintor, J., 2020. Melatonin and the control of intraocular pressure. Prog. Retin. Eye Res. 75.
Artifoni, M., Rothschild, P.R., Brézin, A., Guillevin, L., Puéchal, X., 2013. Ocular inflammatory diseases associated with rheumatoid arthritis. Nat. Rev. Rheumatol. 10 (2), 108–116.
Bantounou, M., Plascevic, J., Galley, H.F., 2022. Melatonin and related compounds: antioxidant and anti-inflammatory actions. Antioxidants . 11 (3), 532.
Baspinar, Y., Borchert, H.H., 2012. Penetration and release studies of positively and negatively charged nanoemulsions—Is there a benefit of the positive charge? Int. J. Pharm. 430 (1–2), 247–252.
Belkhelladi, M., Bougrine, A., 2024. Rosehip extract and wound healing: a review. J. Cosmet. Dermatol. 23 (1), 62–67.
Benedeto-Stojanov, D., Ničković, V.P., Petrović, G., Rancić, A., Grgov, I., Nikolić, G.R., et al., 2024. Melatonin as a promising anti-inflammatory agent in an in vivo animal model of sepsis-induced rat liver damage. Int. J. Mol. Sci. 25 (1), 455.
Bonilla, L., Espina, M., Severino, P., Cano, A., Ettcheto, M., Camins, A., et al., 2022. Lipid nanoparticles for the posterior eye segment. Pharmaceutics. 14 (1), 90.
Bonilla-Vidal, L., Świtalska, M., Espina, M., Souto, E.B., Gliszczyńska, A., Sánchez-López, E.J.G., 2024. Nanostructured lipid carriers co-encapsulating Apigenin and Melatonin: an innovative strategy against cancer. Mater. Des., accepted
Bonilla-Vidal, L., Świtalska, M., Espina, M., Wietrzyk, J., García, M.L., Souto, E.B., et al., 2023. Dually Active Apigenin-Loaded Nanostructured Lipid Carriers for Cancer Treatment. Int. J. Nanomed. 18 (November), 6979–6997.
Bonilla-Vidal, L., Espina, M., García, M.L., Baldomà, L., Badia, J., González, J.A., et al., 2024. Novel nanostructured lipid carriers loading Apigenin for anterior segment ocular pathologies. Int. J. Pharm. 658 (March).
Bonilla-Vidal, L., Espina, M., García, M.L., Cimino, C., Carbone, C., Baldomà, L., et al., 2024. Melatonin loaded nanostructured lipid carriers for the treatment of uveal melanoma. J. Drug Deliv. Sci. Technol.
Bonilla-Vidal, L., Świtalska, M., Espina, M., Wietrzyk, J., García, M.L., Souto, E.B., et al., 2024. Antitumoral melatonin-loaded nanostructured lipid carriers. Nanomedicine 19 (23), 1879–1894.
Bunjes, H., Westesen, K., Koch, M.H.J., 1996. Crystallization tendency and polymorphic transitions in triglyceride nanoparticles. Int. J. Pharm. 129 (1–2), 159–173.
Cavalier, A.N., Clayton, Z.S., Wahl, D., Hutton, D.A., McEntee, C.M., Seals, D.R., et al., 2024. Protective effects of apigenin on the brain transcriptome with aging. Mech. Ageing Dev. 217, 111889.

Cho, J.H., Bhutani, S., Kim, C.H., Irwin, M.R., 2021. Anti-inflammatory effects of melatonin: a systematic review and meta-analysis of clinical trials. Brain Behav. Immun. 93, 245–253.
Colin, J., 2007. The role of NSAIDs in the management of postoperative ophthalmic inflammation. Drugs 67 (9), 1291–1308.
Da Cunha, A.P., Zhang, Q., Prentiss, M., Wu, X.Q., Kainz, V., Xu, Y.Y., et al., 2018. The hierarchy of proinflammatory cytokines in ocular inflammation. Curr. Eye Res. 43 (4), 553–565.
Deng, S.L., Zhang, B.L., Reiter, R.J., Liu, Y.X., 2020. Melatonin ameliorates inflammation and oxidative stress by suppressing the p38MAPK signaling pathway in LPS-induced sheep orchitis. Antioxidants 9 (12), 1–17.
Egwuagu, C.E., Sun, L., Kim, S.-H., Dambuza, I.M., 2015. Ocular inflammatory diseases: molecular pathogenesis and immunotherapy. Curr. Mol. Med. 15 (6), 517–528.
Esteruelas, G., Halbaut, L., García-Torra, V., Espina, M., Cano, A., Ettcheto, M., et al., 2021. Development and optimization of Riluzole-loaded biodegradable nanoparticles incorporated in a mucoadhesive in situ gel for the posterior eye segment. Int. J. Pharm. 612, 121379.
Fangueiro, J.F., Calpena, A.C., Clares, B., Andreani, T., Egea, M.A., Veiga, F.J., et al., 2016. Biopharmaceutical evaluation of epigallocatechin gallate-loaded cationic lipid nanoparticles (EGCG-LNs): In vivo, in vitro and ex vivo studies. Int. J. Pharm. 502 (1), 161–169.
Fernandes, A.R., Vidal, L.B., Sánchez-López, E., dos Santos, T., Granja, P.L., Silva, A.M., et al., 2022. Customized cationic nanoemulsions loading triamcinolone acetonide for corneal neovascularization secondary to inflammatory processes. Int. J. Pharm. 623 (June).
Freitas, C., Müller, R.H., 1998. Effect of light and temperature on zeta potential and physical stability in solid lipid nanoparticle (SLN™) dispersions. Int. J. Pharm. 168 (2), 221–229.
Freitas, C., Müller, R.H., 1999. Correlation between long-term stability of solid lipid nanoparticles (SLN) and crystallinity of the lipid phase. Eur. J. Pharm. Biopharm. 47 (2), 125–132.
Fu, X., Kong, W., Zhang, Y., Jiang, L., Wang, J., Lei, J., 2015. Novel solid–solid phase change materials with biodegradable trihydroxy surfactants for thermal energy storage. RSC Adv. 5 (84), 68881–68889.
Funakoshi-Tago, M., Nakamura, K., Tago, K., Mashino, T., Kasahara, T., 2011. Anti-inflammatory activity of structurally related flavonoids, Apigenin, Luteolin and Fisetin. Int. Immunopharmacol. 11 (9), 1150–1159.
Galindo, R., Elena, S., Espina, M., Ettcheto, M., Cano, A., Haro, I., et al., 2022. Development of Peptide Targeted PLGA-PEGylated Nanoparticles Loading Licochalcone-A for Ocular Inflammation. Pharmaceutics. 14, 285.
Ghasemi, H., Ghazanfari, T., Yaraee, R., Faghihzadeh, S., Hassan, Z.M., 2011. Roles of IL-8 in ocular inflammations: a review. Ocul. Immunol. Inflamm. 19 (6), 401–412.
Gu, W., Wu, M., Cui, S., Bo, J., Wu, H., 2024. Melatonin's protective effects on neurons in an in vitro cell injury model. Discov. Med. 36 (182), 509–517.
Huang, Z., Ma, C., Wu, M., Li, X., Lu, C., Zhang, X., et al., 2020. Exploring the drug-lipid interaction of weak-hydrophobic drug loaded solid lipid nanoparticles by isothermal titration calorimetry. J. Nanoparticle Res. 22 (1), 1–14.
Jung, W.W., 2014. Protective effect of apigenin against oxidative stress-induced damage in osteoblastic cells. Int. J. Mol. Med. 33 (5), 1327–1334.
Kany, S., Vollrath, J.T., Relja, B., 2019. Cytokines in inflammatory disease. Int. J. Mol. Sci. 20 (23), 6008.
Khosa, A., Reddi, S., Saha, R.N., 2018. Nanostructured lipid carriers for site-specific drug delivery. Biomed. Pharmacother. 103, 598–613.
Kopustinskiene, D.M., Bernatoniene, J., 2021. Molecular mechanisms of melatonin-mediated cell protection and signaling in health and disease. Pharmaceutics. 13 (2), 129.
Landh, E., Moir, L.M., Traini, D., Young, P.M., Ong, H.X., 2020. Properties of rapamycin solid lipid nanoparticles for lymphatic access through the lungs & part II: the effect of nanoparticle charge. Nanomedicine 15 (20), 1947–1963.
Lee, R.W.J., Dick, A.D., 2011. Current concepts and future directions in the pathogenesis and treatment of non-infectious intraocular inflammation. Eye 26 (1), 17–28.
Llorente, X., Esteruelas, G., Bonilla, L., Garnica, M., Filgaira, I., Lopez-Ramajo, D., et al., 2023. Riluzole-loaded nanostructured lipid carriers for hyperproliferative skin diseases. Int. J. Mol. Sci., accepted
Lopes, V., Assis, J., Ribeiro, T., de Castro, G., Pacheco, M., Borges, L., et al., 2020. Melatonin loaded lecithin-chitosan nanoparticles improved the wound healing in diabetic rats. Int. J. Biol. Macromol. 162, 1465–1475.
López-García, J., Lehocký, M., Humpolíček, P., Sáha, P., 2014. HaCaT keratinocytes response on antimicrobial atelocollagen substrates: extent of cytotoxicity, cell viability and proliferation. J. Funct. Biomater. 5 (2), 57.
López-Machado, A., Díaz, N., Cano, A., Espina, M., Badía, J., Baldomà, L., et al., 2021. Development of topical eye-drops of lactoferrin-loaded biodegradable nanoparticles for the treatment of anterior segment inflammatory processes. Int. J. Pharm. 609, 121188.
López-Machado, A., Díaz-Garrido, N., Cano, A., Espina, M., Badia, J., Baldomà, L., et al., 2021. Development of lactoferrin-loaded liposomes for the management of dry eye disease and ocular inflammation. Pharmaceutics 13 (10), 1698.
Mahor, A.K., Singh, P.P., Gupta, R., Bhardwaj, P., Rathore, P., Kishore, A., et al., 2023. Nanostructured lipid carriers for improved delivery of therapeutics via the oral route. J. Nanotechnol. 2023 (1), 4687959.
Mármol, I., Sánchez-De-Diego, C., Jiménez-Moreno, N., Ancín-Azpilicueta, C., Rodríguez-Yoldi, M., 2017. Therapeutic applications of rose hips from different Rosa species. Int. J. Mol. Sci. 18 (6), 1137.
Mazet, R., Yaméogo, J.B.G., Wouessidjewe, D., Choisnard, L., Gèze, A., 2020. Recent advances in the design of topical ophthalmic delivery systems in the treatment of ocular surface inflammation and their biopharmaceutical evaluation. Pharmaceutics 12 (6), 570.
Mofidfar, M., Abdi, B., Ahadian, S., Mostafavi, E., Desai, T.A., Abbasi, F., et al., 2021. Drug delivery to the anterior segment of the eye: A review of current and future treatment strategies. Int. J. Pharm. 607, 120924.
Musa, M., Chukwuyem, E., Ojo, O.M., Topah, E.K., Spadea, L., Salati, C., et al., 2024. Unveiling ocular manifestations in systemic lupus erythematosus. J. Clin. Med. 13 (4), 1047.
Mushtaq, Z., Sadeer, N.B., Hussain, M., Mahwish, A.SA., Imran, M., et al., 2023. Therapeutical properties of apigenin: a review on the experimental evidence and basic mechanisms. Int. J. Food Prop. 26 (1), 1914–1939.
Ojo, A.T., Ma, C., Lee, P.I., 2020. Elucidating the effect of crystallization on drug release from amorphous solid dispersions in soluble and insoluble carriers. Int. J. Pharm. 591, 120005.
Rigas, B., Huang, W., Honkanen, R., 2020. NSAID-induced corneal melt: clinical importance, pathogenesis, and risk mitigation. Surv. Ophthalmol. 65 (1), 1–11.
Sánchez-López, E., Esteruelas, G., Ortiz, A., Espina, M., Prat, J., Muñoz, M., et al., 2020. Dexibuprofen biodegradable nanoparticles: One step closer towards a better ocular interaction study. Nanomaterials 10 (4), 1–24.
Schalnus, R., 2003. Topical nonsteroidal anti-inflammatory therapy in ophthalmology. Ophthalmologica 217 (2), 89–98.
Silva, A.M., Martins-Gomes, C., Fangueiro, J.F., Andreani, T., Souto, E.B., 2019. Comparison of antiproliferative effect of epigallocatechin gallate when loaded into cationic solid lipid nanoparticles against different cell lines. Pharm. Dev. Technol. 24 (10), 1243–1249.
Souto, E.B., Mehnert, W., Müller, R.H., 2006. Polymorphic behaviour of Compritol 888 ATO as bulk lipid and as SLN and NLC. J. Microencapsul. 23 (4), 417–433.
Souto, E.B., Doktorovova, S., Gonzalez-Mira, E., Egea, M.A., Garcia, M.L., 2010. Feasibility of lipid nanoparticles for ocular delivery of anti-inflammatory drugs. Curr. Eye Res. 35 (7), 537–552.
Starace, V., Battista, M., Brambati, M., Cavalleri, M., Bertuzzi, F., Amato, A., et al., 2021. The role of inflammation and neurodegeneration in diabetic macular edema. Ther. Adv. Ophthalmol. 13, 25158414211055964.
Strugała, P., Gładkowski, W., Kucharska, A.Z., Sokół-Łetowska, A., Gabrielska, J., 2016. Antioxidant activity and anti-inflammatory effect of fruit extracts from blackcurrant, chokeberry, hawthorn, and rosehip, and their mixture with linseed oil on a model lipid membrane. Eur. J. Lipid Sci. Technol. 118 (3), 461–474.
Tarocco, A., Caroccia, N., Morciano, G., Wieckowski, M.R., Ancora, G., Garani, G., et al., 2019. Melatonin as a master regulator of cell death and inflammation: molecular mechanisms and clinical implications for newborn care. Cell Death Dis. 10 (4), 1–12.
Thiruchenthooran, V., Świtalska, M., Bonilla, L., Espina, M., García, M.L., Wietrzyk, J., et al., 2022. Novel strategies against cancer: dexibuprofen-loaded nanostructured lipid carriers. Int. J. Mol. Sci. 23 (19), 11310.
Thiruchenthooran, V., Espina, M., Świtalska, M., Bonilla, L., Wietrzyk, J., García, M.L., et al., 2024. Combination of indomethacin with nanostructured Lipid carriers for effective anticancer therapy. Int. J. Nanomed. (July) (In revision).
Vedadghavami, A., Zhang, C., Bajpayee, A.G., 2020. Overcoming negatively charged tissue barriers: Drug delivery using cationic peptides and proteins. Nano Today 34.
Wang, J., Liao, Y., Fan, J., Ye, T., Sun, X., Dong, S., 2012. Apigenin inhibits the expression of IL-6, IL-8, and ICAM-1 in DEHP-Stimulated human umbilical vein endothelial cells and in vivo. Inflammation 35 (4), 1466–1476.
Wang, J.J., Sung, K.C., Hu, O.Y.P., Yeh, C.H., Fang, J.Y., 2006. Submicron lipid emulsion as a drug delivery system for nalbuphine and its prodrugs. J. Control. Release 115 (2), 140–149.
Wong, C.W., Wong, T.T., 2019. Posterior segment drug delivery for the treatment of exudative age-related macular degeneration and diabetic macular oedema. Br. J. Ophthalmol. 103 (10), 1356–1360.
Xu, H., Rao, N.A., 2022. Grand challenges in ocular inflammatory diseases. Front. Ophthalmol. 2, 756689.
Yang, W., Wang, L., Mettenbrink, E.M., Deangelis, P.L., Wilhelm, S., 2021. Nanoparticle toxicology. Annu. Rev. Pharmacol. Toxicol. 61, 269–289.
Yoon, J.H., Kim, M.Y., Cho, J.Y., 2023. Apigenin: a therapeutic agent for treatment of skin inflammatory diseases and cancer. Int. J. Mol. Sci. 24 (2), 1498.
Yue, T., Shi, Y., Luo, S., Weng, J., Wu, Y., Zheng, X., 2022. The role of inflammation in immune system of diabetic retinopathy: Molecular mechanisms, pathogenetic role and therapeutic implications. Front. Immunol. 13, 1055087.
Zarezadeh, M., Khorshidi, M., Emami, M., Janmohammadi, P., Kord-varkaneh, H., Mousavi, S.M., et al., 2020. Melatonin supplementation and pro-inflammatory mediators: a systematic review and meta-analysis of clinical trials. Eur. J. Nutr. 59 (5), 1803–1813.
Zhang, W., Li, X., Ye, T., Chen, F., Yu, S., Chen, J., et al., 2014. Nanostructured lipid carrier surface modified with Eudragit RS 100 and its potential ophthalmic functions. Int. J. Nanomed. 9, 4315.
Zhang, J., Liu, D., Huang, Y., Gao, Y., Qian, S., 2012. Biopharmaceutics classification and intestinal absorption study of apigenin. Int. J. Pharm. 436 (1–2), 311–317.
Zimmermann, E., Souto, E.B., Müller, R.H., 2005. Physicochemical investigations on the structure of drug-free and drug-loaded solid lipid nanoparticles (SLN) by means of DSC and 1H NMR. Pharmazie 60 (7), 508–513.